Angular distribution of δ electrons emitted in collisions of 1.0-MeV/u F^{q+} ($q = 4, 6, 8, 9$) with molecular hydrogen

C. Liao, P. Richard, S. R. Grabbe, C. P. Bhalla, T. J. M. Zouros,* and S. Hagmann
J. R. Macdonald Laboratory, Department of Physics, Kansas State University, Manhattan, Kansas 66506-2604
(Received 16 December 1993)

The angular distribution, as well as the energy distribution of δ electrons produced in collisions of 1.0-MeV/u F^{q+} ($q = 4, 6, 8, 9$) ions with molecular hydrogen, have been studied for laboratory observation angles (θ_L) from 0° to 70° with respect to the beam direction. The measurements are in fair agreement with the impulse approximation calculations which use the quantal elastic electron-ion differential scattering cross sections folded with the Compton profile of the target electrons. We observe that the energy of the centroid of the binary-encounter-electron (BEE) peak is projectile charge state, q, and laboratory angle, θ_L, dependent. Moreover, at 0°, an enhancement of the ratio of the observed double differential cross section for nonbare projectiles to that for the bare ion projectiles, $\sigma(q+)/\sigma(9+)$, is observed, contrary to the q^2 scaling predicted by a first Born calculation for ionization. This ratio $\sigma(q+)/\sigma(9+)$ decreases monotonically with increasing θ_L, and becomes smaller than one for $\theta_L \geq 30°$.

PACS number(s): 34.50.Fa

I. INTRODUCTION

Ion-atom collisions lead to the copious emission of electrons with energies from approximately zero up to many keV. It is well established that spectra of continuous energy electrons (so called δ electron) emitted in swift ion-atom collisions, generally exhibit three distinct prominent features [1–3]: (1) a strong and monotonically decreasing continuum of electrons due to soft collisions between projectile and target electrons. This feature of the spectrum, particularly at large laboratory observation angles, θ_L, may appear to dominate the entire spectrum; (2) a strong sharp prominent cusp or equal velocity ($V_e = V_p$, where V_e and V_p are the target electron and projectile velocities, respectively) peak at 0° with respect to the beam direction ($\theta_L = 0°$). This contains electron loss from the projectile to the continuum (ELC) and electron capture from the target atom to the continuum of the projectile contributions. At nonzero observation angles ($\theta_L \neq 0°$) this peak is seen as a broad electron loss peak; and (3) a broad peak, the binary-encounter-electron (BEE) peak which is due to target electrons ionized through direct, hard collisions with the projectiles. Using elastic two-body collision dynamics for heavy-ion impact on a free electron, the scattered electron velocity is $V_e = 2V_p \cos\theta_L$, the energy of this scattered electron is thus $E_{\mathrm{BEE}} = 4E_p(m_e/M_p)\cos^2\theta_L$ ($0° \leq \theta_L \leq 90°$), where E_p is the projectile energy and m_e/M_p is the electron to projectile mass ratio.

Binary encounter electrons have recently been extensively studied [4–15]. Most of the investigations, however, have concentrated on the forward direction and in particular at $\theta_L = 0°$. Some measurements of the angular dependence have also been reported [3,10–15].

For bare-ion-atom collisions, Lee *et al.* [4] used a variety of 1–2 MeV/u bare ions (H^+, C^{6+}, N^{7+}, O^{8+}, and F^{9+}) in collisions with H_2 and He targets to study BEE production at $\theta_L = 0°$, the double differential cross section (DDCS) was found to be in excellent agreement with the Z^2-scaling law (where Z is the incident projectile charge), which was derived from first-order perturbation theory. The energy of the BEE peak was observed to be shifted to a lower energy than the "classical" two-body free electron energy value, E_{BEE}. This shift was explained to be due to the effect of the binding energy of the target electron. For large θ_L, however, Pedersen *et al.* [5] investigated DDCS for ejection of electrons from helium by different projectiles (1.00 and 1.84 MeV/u H^+, He^{2+}, C^{6+}, and O^{8+}) at different θ_L, and found large departures from the Z^2 dependence of the cross section, particularly above and below the binary encounter peak. The deviations were explained to be due to the simultaneous effect of the projectile and residual target fields.

For non-bare-ion-atom collisions, Richard *et al.* [6] reported that the double differential BEE cross section at $\theta_L = 0°$ in collisions of 1.0 and 1.5 MeV/u $F^{(3-9+)}$ with H_2 and He targets increases with decreasing projectile charge state, which is in contradiction to the q^2-scaling law predicted by a first Born approximation. This result was also confirmed in electron-projectile coincidence experiments [7,8], where the pure target ionization channel was selected.

In the impulse approximation (IA), the ionization of target electrons in ion-atom collisions is treated as elastic scattering of quasifree target electrons from the screened projectile potential. The theoretical DDCS for BEE emission is then obtained by folding this calculated differential elastic scattering cross section with the Comp-

*Present address: Department of Physics, University of Crete & Institute of Electronic Structure and Lasers, P.O. Box 1527, 711 10, Heraklion, Crete, Greece.

ton profile of the target electrons. By using the static screened potential and the impulse approximation, several calculations of good agreement with the experimental data were reported [16,17] for the BEE region. Miraglia and Macek [18] had performed calculations using various models applicable to the entire electron emission region and compared to the data. Taulbjerg [19] and Bhalla and Shingal [20] found that inclusion of electron exchange between the quasifree target electrons and the projectile electrons gives an improved agreement between experiment and theory. Classical trajectory Monte Carlo calculations also gives non-q^2 scaling of the ionization cross section [21,22].

Recently the angular dependence of the BEE production, as well as the energy shift of BEE peak, for different charge states of carbon projectiles were measured, and part of these data were compared with calculations [14,15] based on a distorted-wave methods. However, in their experiment, only the ratio of the DDCS for non-bare ion to bare ion were investigated from 3° to 60° in the laboratory frame, the comparison between absolute cross sections at different angles was therefore not possible. Several angular distribution studies using much heavier projectiles have also been reported [10–13], an anomalous oscillation in the ejected electron spectrum in the binary peak region was observed. The observed structures were attributed to diffractive scattering of the target quasifree electrons in the projectile potential.

It is the purpose of this paper to report on the studies of the angular distribution of δ electrons, with particular emphasis on the BEE, emitted in 1.0 MeV/u F^{q+} ($q = 4, 6, 8, 9$) on molecular hydrogen with θ_L between 0° and 70°. A comparison of absolute electron production cross section, as well as the energy of the BEE peak, at different observation angles and different projectile charge states are presented. Following the brief discussion of experimental method in Sec. II, IA calculations of the BEE production will be introduced in Sec. III. Section IV is devoted to comparisons of the experimental and theoretical cross sections.

II. EXPERIMENTAL METHOD

A. Technique

A beam of fluorine ions of charge state $q = 4+$ from the EN Tandem Van de Graaff of the J. R. Macdonald Laboratory at Kansas State University was accelerated to an energy of 1.0 MeV/u. After poststripping in 10-μg/cm^2 C foils (for direct beam $q = 4+$, no poststripper foil is needed), the beam was magnetically charge state selected to $q = 4+, 6+, 8+$, and 9+. On the way to the target gas region the beam was passed through two magnetic quadrupoles and a magnetic deflector, and was tightly collimated over a length of 7.75 m by three adjustable four-jaw slit systems (typically open to 3x3 mm^2, 1x1 mm^2, and 1.2x1.2 mm^2), the last one serving as a beam scraper to reduce slit edge scattering. The hydrogen gas was brought into the separately pumped interaction region through a hypodermic needle ($d = 0.5$ mm) (see Fig. 1). The target gas pressure was kept constant within 2%, and single collision conditions have been verified experimentally.

The electrons emitted into a solid angle of 2.5x10^{-3} sr were energy analyzed with an electrostatic hemispherical electron analyzer ($R_0 = 160$ mm) and then detected by a channel electron multiplier. The spectrometer was mounted on a frame, which can be externally rotated around the center of the chamber, where the gas jet was located. The energy resolution of the spectrometer was set to 2%. The scattering chamber has been equipped with a double μ metal shielding to isolate the collision region and the spectrometer from magnetic fields. The measured magnetic field was smaller than 2 mG. A shielded Faraday cup was used to measure the beam current, which was used to normalize the electron count for each electron energy channel.

Considerable care was taken in reducing the beam-induced background by carefully collimating the beam. Such a background can be a large source of error, especially at smaller observation angles, due to their longer target length. This beam-induced electron background was directly determined by taking an electron spectrum without gas in the gas jet, and then subtracted from the electron spectrum with target gas in the gas jet.

B. Data evaluation

We obtained an energy calibration of our spectrometer using Ne K Auger and Ar L Auger electrons from collisions 3 MeV H^++Ne,Ar, since the energies of these target Auger electrons are well known [23,24].

For a correct derivation of the DDCS of BEE from the data, it has been found that a precise knowledge of the beam velocity is indispensable [25], hence a precise measurement of the projectile energy is required. The determination of the cusp energy has been found to be a convenient and reliable way [26] of measuring the actual projectile velocities to within 0.1%. The cusp energy can be determined experimentally by directly measuring its value in the electron spectrum at $\theta_L = 0°$. For highly charged ions obtained by poststripping projectile ions of a lower charge state, a small but observable energy loss of the beam occurs as it traverses the poststripper foil.

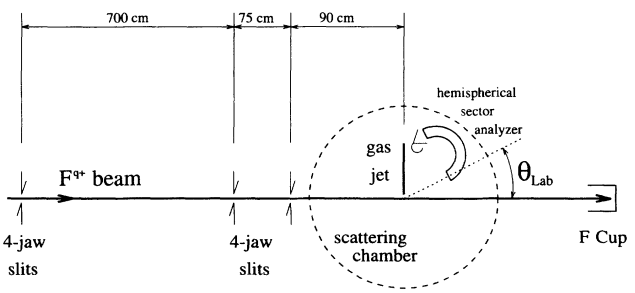

FIG. 1. Experimental setup to measure angular and energy distribution of δ electrons. The double focusing hemispherical sector analyzer can be rotated to detect electrons emitted from 0° to 70° with respect to the beam axis.

This effect is accounted for in our data by measuring the 0° cusp energy for all the charge states.

The experimental DDCS for electron production in ion-atom collisions can be obtained from the expression

$$\frac{d^2\sigma}{dEd\Omega}(E,\theta_L) = \frac{N_e(E,\theta_L)}{N_p n l(\theta_L)\Delta E \Delta\Omega \eta(E)}, \quad (1)$$

where $N_e(E,\theta_L)$ is the detected electron count at a given electron energy E and a given observation angle θ_L, N_p is the number of incoming projectiles, which can be derived from the beam current (measured by a Faraday cup) and projectile charge state, n is the target density, which is proportional to the pressure in the scattering chamber, $l(\theta_L)$ is the effect target length at θ_L, ΔE is the spectrometer acceptance energy at electron energy E, which is proportional to electron energy E, $\Delta\Omega$ is the effective solid angle, and $\eta(E)$ is the efficiency of the electron spectrometer.

In our measurement, the factor $n\Delta E\Delta\Omega/E$ is a constant. The channeltron detection efficiency, which is included in $\eta(E)$, is a known function of electron energy E [27], but is taken as energy independent in the electron energy region studied here. Since Ne K Auger lines excited by protons are known to be isotropic to better than 3%, the Ne K Auger cross sections for 3 MeV p+Ne collisions were measured at different θ_L, and were used to obtain a target length correction as a function of θ_L. At large observation angles ($\theta_L > 15°$), our target length correction is consistent with a $\frac{1}{\sin\theta_L}$ correction.

III. CALCULATION OF DDCS FOR BEE

The impulse approximation is expected to be valid when the velocity of the incoming ion projectile is much larger than the orbital velocity of the target electron, as is the case for the collision systems considered here. Within the impulse approximation, the BEE production cross section can be related to the differential cross section for the electron-ion elastic scattering [see Eq. (6) below].

The spherically symmetric potential of the ion consists of the static potential, $V_s(r)$, due to the interaction of the incident electrons with the nucleus and the electrons of the ion, A^{q+}, and asymptotically is given by $-q/r$. In addition to the static potential, the nonlocal exchange contribution, $\chi_l(r)$, due to the interaction of the continuum and bound orbitals is incorporated. The radial wave function $u_l(r)$ of the scattered state of the incident electron (energy $E = k^2/2$ and orbital angular momentum l) is a solution of the second-order coupled integro-differential equation of the form

$$\left(\frac{d^2}{dr^2} - \frac{l(l+1)}{r^2} - 2V_s(r) + k^2\right) u_l(r) = \chi_l(r). \quad (2)$$

The scattering amplitude for such a potential can be expressed as

$$f(\theta) = f_c(\theta) + f_s(\theta), \quad (3)$$

where $f_c(\theta)$ is the static Coulomb scattering amplitude for the asymptotic charge q and $f_s(\theta)$ is the scattering amplitude that includes both V_s and the exchange contributions,

$$f_s(\theta) = (2ik)^{-1}\sum_{l=0}^{\infty}(2l+1)\exp(2i\sigma_l) \times[\exp(2i\delta_l) - 1]P_l(\cos\theta), \quad (4)$$

where σ_l is the Coulomb phase shift for the asymptotic charge q and δ_l is the additional phase shift due to screening and exchange effects.

The static potential, V_s, the nonlocal exchange contribution, χ_l, and the radial wave function, $u_l(r)$, were calculated in a self-consistent Hartree-Fock atomic model. The phase shifts were calculated up to a maximum l value beyond which there was negligible contributions to the scattering amplitude. Where appropriate, the phase shifts were calculated for both singlet (S) and triplet (T) cases, and the differential elastic scattering cross sections were obtained as follows:

$$\frac{d\sigma(\theta)}{d\Omega} = \frac{1}{4}\left(\frac{d\sigma_S(\theta)}{d\Omega} + 3\frac{d\sigma_T(\theta)}{d\Omega}\right). \quad (5)$$

The double differential electron production cross section in the ion-atom collision can be related to DCS in the electron-ion collision through the IA. In the projectile rest frame,

$$\frac{d^2\sigma(E,\theta)}{dEd\Omega} = \left(\frac{d\sigma(\theta)}{d\Omega}\right)\left(\frac{J(|p_z|)}{V_p + p_z}\right), \quad (6)$$

where $J(|p_z|)$ is the Compton profile of the target atom with $p_z = \sqrt{2(E+E_b)} - V_p$. Here E_b is the binding energy of the electron.

The DDCS of BEE in the laboratory frame are obtained by the standard transformation [28]

$$\frac{d^2\sigma_L(E_L,\theta_L)}{dE_L d\Omega_L} = \left(\frac{E_L}{E}\right)^{\frac{1}{2}}\frac{d^2\sigma(E,\theta)}{dEd\Omega}, \quad (7)$$

where E_L and θ_L are, respectively, the electron energy in the laboratory frame and the electron emission angle with respect to the incident projectile direction

$$E_L = \frac{1}{2}[V_p\cos\theta_L + (2E - V_p^2\sin^2\theta_L)^{\frac{1}{2}}]^2, \quad (8)$$

$$\cos\theta = \frac{V_p - (2E_L)^{\frac{1}{2}}\cos\theta_L}{[2E_L + V_p^2 - 2V_p(2E_L)^{\frac{1}{2}}\cos\theta_L]^{\frac{1}{2}}}. \quad (9)$$

IV. EXPERIMENTAL RESULTS AND DISCUSSION

The angular distribution of δ electron production can be presented in three ways.

(a) DDCS as a function of the laboratory observation angle θ_L, providing the comparison between absolute cross sections at different angles for a certain charge state projectile.

(b) DDCS as a function of the projectile charge states, which can be represented by the ratio of DDCS for nonbare projectile to bare ion, yielding the charge state dependence of the electron production at a certain emission angle θ_L.

(c) The BEE peak energy shift from the "classical" two-body free electron energy value, E_{BEE}, as a function of charge state q, and observation angle θ_L, indicating the energy dependence of the BEE peak observed at different observation angles for different projectile charge states.

For the purpose of convenient graphical display, the laboratory frame DDCS in all figures are multiplied by the laboratory electron energy. This quantity is proportional to the measured electron yield.

Figures 2–5 show the laboratory frame electron production for collisions of F^{q+} on H_2 (q=4, 6, 8, and 9) at eight different angles θ_L. All of the data are normalized to the theoretical result of F^{9+} on H_2 at the peak of the BEE yield for $\theta_L = 0°$ (see Fig. 5). Three prominent features can be found in these spectra: a low energy soft electron distribution, a strong cusp at $\theta_L \approx 0°$, and a broad BEE peak.

Low energy electrons are produced in double scattering collisions [29], whereas BEE are generated in binary hard collisions between projectile ions and quasifree target electrons. At small observation angles θ_L, the BEE peak is clearly distinguishable, however, with increasing θ_L, the BEE peak is strongly shifted to lower energies.

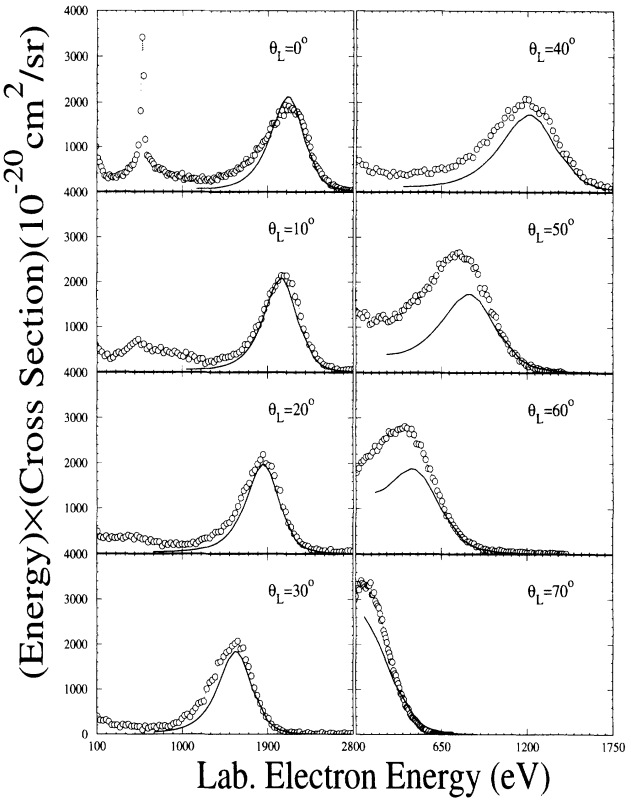

FIG. 3. Same as Fig. 2, but for the collisions of $F^{6+}+H_2$.

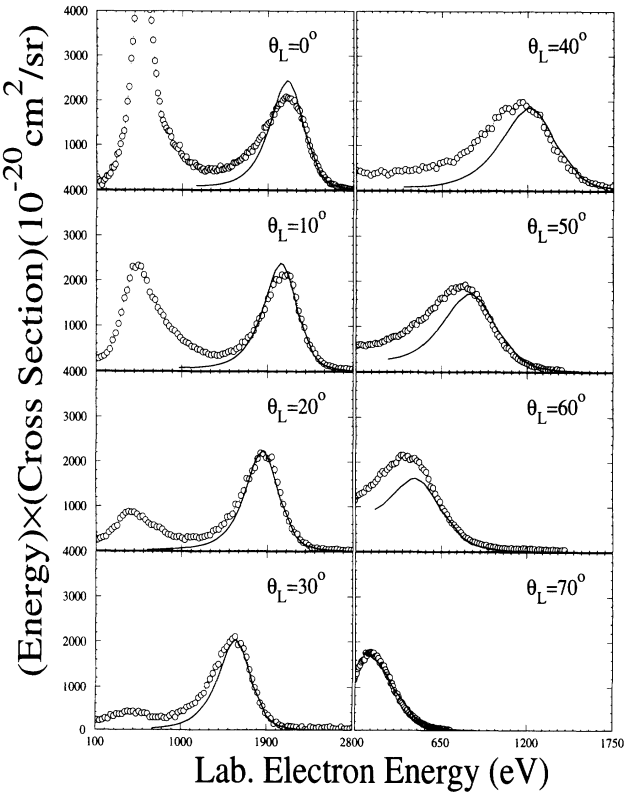

FIG. 2. Laboratory cross section times laboratory electron energy for electron production in 1.0 MeV/u $F^{4+}+H_2$ collisions. Solid lines are the results of the impulse approximation. The observation angle θ_L is varied as indicated.

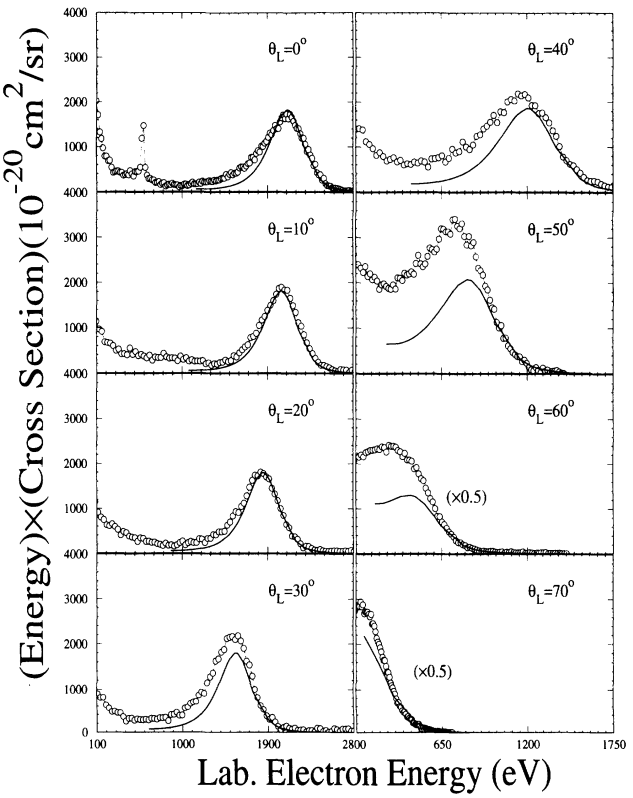

FIG. 4. Same as Fig. 2, but for the collisions of $F^{8+}+H_2$. For the purpose of convenient graphical display, at $\theta_L = 60°$ and 70°, both experimental data and theoretical results are divided by a factor of 2.

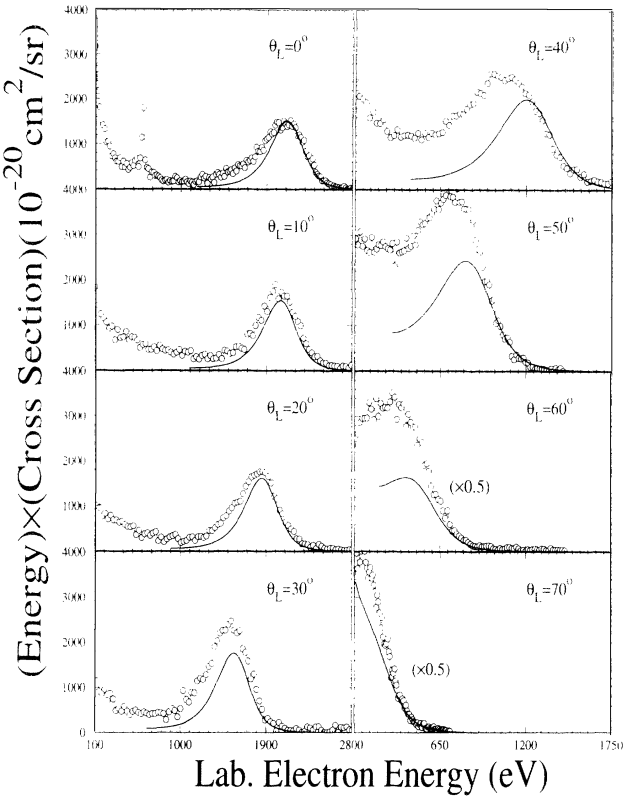

FIG. 5. Same as Fig. 4, but for the collisions of $F^{9+}+H_2$.

Classically it is given by $E_{\mathrm{BEE}} = 4E_p(m_e/M_p)\cos^2\theta_L$ ($0° \leq \theta_L \leq 90°$). At $\theta_L = 60°$, E_{BEE} gives the same value as the $V_e = V_p$ peak, and therefore the BEE peak cannot be clearly identified. Beyond this observation angle, a reasonable comparison between experiment and theory is not feasible.

Theoretical results for the BEE production calculated in the impulse approximation, as discussed in Sec. III, are shown in Figs. 2–5 as solid lines. For small θ_L ($\theta_L \leq 30°$), the agreement between the data and the calculation is good. At larger θ_L, however, this agreement is not so good. We attribute the difference between the experimental data and the theoretical calculation mainly to the high energy tail of the ELC and double scattering soft electron contributions. The impulse approximation is not applicable to the production of these low energy electrons.

In our experiments, the energy of the centroid of the BEE peak is observed to be shifted to a lower energy than the "classical" two-body free electron energy value, E_{BEE}. This energy shift is both projectile charge state and laboratory observation angle dependent. Figure 6 shows the measured energy shift of the BEE peak from the two-body free electron value as a function of θ_L in the angular range where the BEE peak can be distinguished from the soft electron background (i.e., from 0° to 50°). The measured shifts increase with increasing observation angle θ_L and are projectile charge state q dependent; however, the errors in extracting this shift become significantly larger for the large angles. The impulse approximation model, based on the energy and momentum

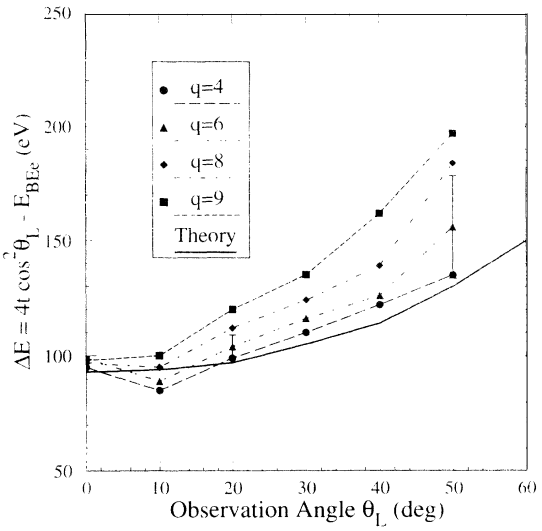

FIG. 6. The energy shift of the BEE peak in 1.0 MeV/u $F^{q+}+H_2$ collisions as a function of observation angles θ_L. Solid line is the results of the impulse approximation. q is varied as indicated.

conservation in which the binding energy E_b of the target electron enters, gives the prediction that the energy shift of the BEE peak is target dependent (at $\theta_L = 0°$, it was confirmed by Lee *et al.* [4]), but q independent. The present data show a strong q dependence for large observation angles. The Bohr and Lindhard (BL) model, which was used in the work of Pedersen *et al.* [5], however, assumes that the electron is released when the force from the projectile field balances that of the target field, and predicts that the energy shift of BEE is target and q dependent (proportional to $\sqrt{q}$), but still θ_L independent. The measured values of ΔE in the present experiment show negligible variation with q at 0° and show a consistent increasing with q for all other angles, but due to the large error in the values of ΔE, no meaningful q dependence can be extracted. Similar results are obtained for carbon ion projectiles by González *et al.* [14,15]; Hidmi *et al.* [30] also observed non $\sqrt{q}$ dependence at 0° for a large range of projectile Z. It is noted that the BL model favors slow collisions, since the electrons do not have enough time to adjust themselves to the potential of the projectile during the high velocity collisions studied here. The IA model and the continuum-distorted-wave

TABLE I. The ratio of electron production at the BEE peak for nonbare projectiles to the bare projectile in 1.0 MeV/u $F^{q+}+H_2$ collisions.

Angle	Experiment			Theory		
θ_L	$q=4$	$q=6$	$q=8$	$q=4$	$q=6$	$q=8$
0°	1.38	1.28	1.15	1.62	1.41	1.21
10°	1.29	1.22	1.08	1.55	1.36	1.18
20°	1.22	1.17	1.01	1.38	1.22	1.11
30°	0.84	0.85	0.89	1.15	1.04	1.02
40°	0.77	0.81	0.86	0.92	0.87	0.93
50°	0.49	0.69	0.85	0.71	0.71	0.85
60°	0.30	0.40	0.68	0.50	0.57	0.79

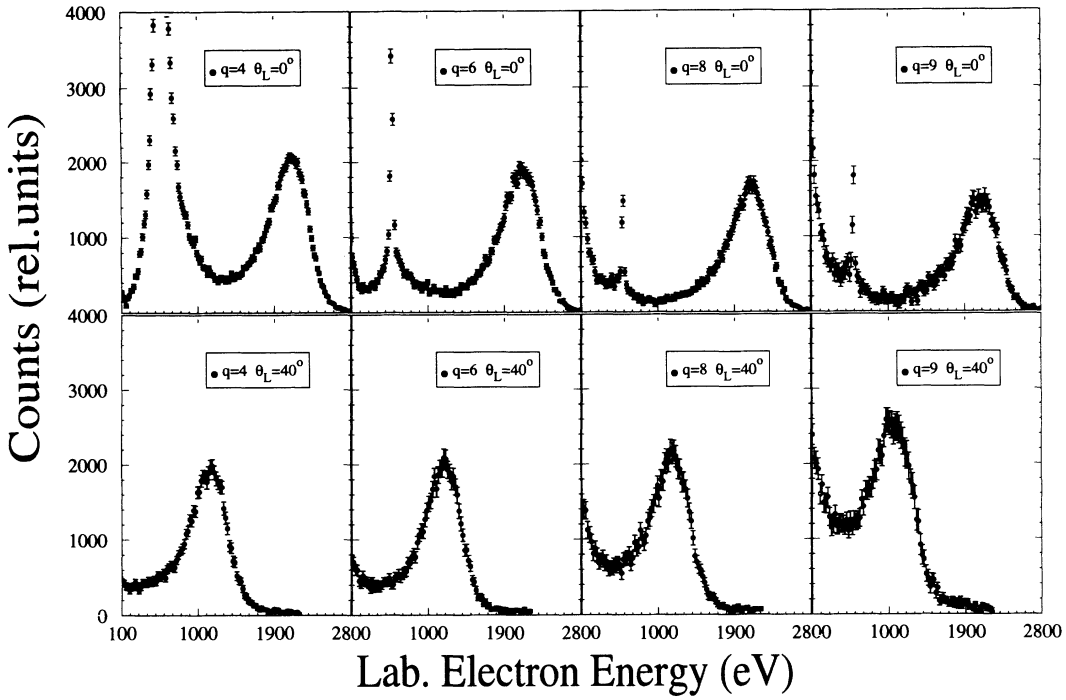

FIG. 7. Electron energy spectra for the collision of 1.0 MeV/u $F^{q+}+H_2$ at 0° and 40° observation angles. The projectile charge state q is varied as indicated. The error bars are calculated from statistics alone. The cross section decreases with increasing q for the $\theta_L = 0°$ data and increases with increasing q for the $\theta_L = 40°$ data.

eikonal-initial-state calculations both give a weak θ_L dependence but fall below the observed energy shifts for large θ_L.

The BEE production is also observed to be both q and θ_L dependent. At small observation angles, the measured BEE production decreases with increasing projectile charge state q, i.e., with decreasing number of projectile electrons, contrary to the q^2-scaling law predicted by a first Born approximation. However, this q dependence varies with increasing θ_L. At large observation angles ($\theta_L \geq 30°$), the BEE production is observed to increase with increasing charge state q, and this increasing becomes stronger for larger θ_L (see Table I). The q dependence of BEE production for two observation angles ($\theta_L = 0°$ and 40°) is shown in Fig. 7.

The ratio of δ electron production in collisions of $F^{4+}+H_2$ to that in collisions of $F^{9+}+H_2$, $R = \frac{d^2\sigma}{dEd\Omega}(q = 4)/\frac{d^2\sigma}{dEd\Omega}(q = 9)$, is plotted in Fig. 8 as a function of electron energy for different angles. In the high energy region, this ratio R decreases with increasing θ_L, indicating the angular dependence of the enhancement. In the low energy region, however, the ELC peak appears prominently and tends to obscure the analysis at forward direction. The ELC peak decreases rapidly with increasing θ_L and disappears at $\theta_L > 40°$. The ratio R is observed to be smaller than one, predicted by Z^2 scaling, but larger than $(4/9)^2 = 0.20$, predicted by the q^2 scaling law from the first Born approximation, showing that the screening of the projectile electrons is significant [31]. As pointed out by Stolterfoht *et al.* [31], the full screening is observed for low energy electrons where the adiabatic radius, $R_{ab} = \hbar V_p/Q$, is larger than 1, where

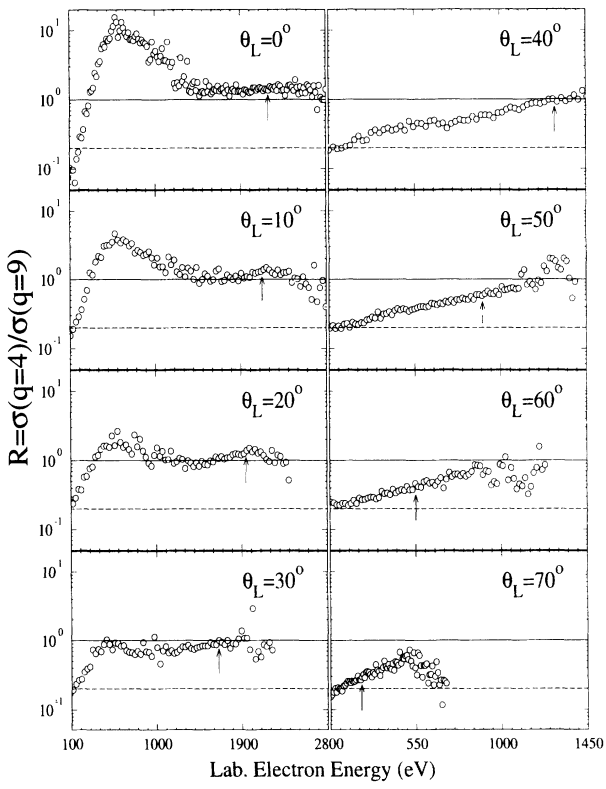

FIG. 8. The ratio of electron production for nonbare projectile F^{4+} to bare projectile F^{9+} in 1.0 MeV/u $F^{q+}+H_2$ collisions. Solid line, Z^2 scaling prediction; broken line, first Born approximation prediction. Arrow indicates E_{BEE}. The observation angle θ_L is varied as indicated.

V_p is projectile velocity and $Q = E + E_b$. In the very low electron energy region, $E \sim 100$ eV, corresponding to distant collisions, we find the ratio R to be even smaller than 0.2. This is presently investigated in detail using electron-scattered projectile coincidence techniques and will be reported elsewhere.

V. CONCLUSIONS

In summary, the angular distribution, as well as the energy distribution of δ electrons produced in collisions of 1.0 MeV/u F^{q+} (q=4,6,8,9) ions with H_2 has been studied from 0° to 70° with respect to the beam direction. Three prominent features of the electron spectra are discussed. The enhancement and screening effects are observed at different laboratory observation angles. At small θ_L, the experimental data are found to be in good agreement with the calculation based upon the impulse approximation. At larger θ_L, some divergence between experimental and theoretical results is observed; we attribute this divergence mainly to the approximations used in the theoretical methods. The energy shift of the BEE peak, however, is found to be both projectile charge state and observation angle dependent.

ACKNOWLEDGMENTS

We would like to acknowledge the support by the Division of Chemical Sciences, Office of Basic Energy Sciences, Office of Energy Research, U.S. Department of Energy. One of us (T.J.M.Z.) would like to acknowledge the support of NATO Collaborative Research Grant No. CRG-910567.

[1] M. E. Rudd and J. H. Macek, Case Stud. At. Phys. **3**, 47 (1972).
[2] J. H. Macek, Phys. Rev. A **1**, 235 (1970).
[3] N. Stolterfoht, D. Schneider, D. Burch, H. Wieman, and J. S. Risley, Phys. Rev. Lett. **33**, 59 (1974).
[4] D. H. Lee, P. Richard, T. J. M. Zouros, J. M. Sanders, J. L. Shinpaugh, and H. Hidmi, Phys. Rev. A **41**, 4816 (1990).
[5] J. O. P. Pedersen, P. Hvelplund, A. G. Petersen, and P. D. Fainstein, J. Phys. B **24**, 4001 (1991).
[6] P. Richard, D. H. Lee, T. J. M. Zouros, J. M. Sanders, and J. L. Shinpaugh, J. Phys. B **23**, L213 (1990).
[7] T. B. Quinteros, A. D. González, O. Jagutzki, A. Skutlartz, D. H. Lee, S. Hagmann, P. Richard, C. Kelbch, S. L. Varghese, and H. Schmidt-Böcking, J. Phys. B **24**, 1377 (1991).
[8] O. Jagutzki, S. Hagmann, H. Schmidt-Böcking, R. E. Olson, D. R. Schultz, R. Dörner, R. Koch, A. Skutlartz, A. González, T. B. Quinteros, C. Kelbch, and P. Richard, J. Phys. B **24**, 2579 (1991).
[9] P. Hvelplund, H. Tawara, K. Komaki, Y. Yamazaki, K. Kuroki, H. Watanabe, K. Kawatsura, M. Sataka, M. Imai, Y. Kanai, T. Kambara, and Y. Awaya, J. Phys. Soc. Jpn. **60**, 3675 (1990).
[10] C. Kelbch, R. E. Olson, S. Schmidt, H. Schmidt-Böcking, and S. Hagmann, J. Phys. B **22**, 2171 (1989).
[11] S. Hagmann, W. Wolff, J. L. Shinpaugh, H. E. Wolf, R. E. Olson, C. P. Bhalla, R. Shingal, C. Kelbch, R. Herrmann, O. Jagutzki, R. Dörner, R. Koch, J. Euler, U. Ramm, S. Lencinas, V. Dangendorf, M. Unverzagt, R. Mann, P. Mokler, J. Ullrich, H. Schmidt-Böcking, and C. L. Cocke, J. Phys. B **25**, L287 (1992).
[12] W. Wolff, J. L. Shinpaugh, H. E. Wolf, R. E. Olson, J. Wang, S. Lencinas, D. Piscevic, R. Herrmann, and H. Schmidt-Böcking, J. Phys. B **25**, 3683 (1992).
[13] W. Wolff, J. L. Shinpaugh, H. E. Wolf, R. E. Olson, U. Bechthold, and H. Schmidt-Böcking, J. Phys. B **26**, L65 (1993).
[14] A. D. González, P. Dahl, P. Hvelplund, and K. Taulbjerg, J. Phys. B **25**, L573 (1992).
[15] A. D. González, P. Dahl, P. Hvelplund, and P. D. Fainstein, J. Phys. B **26**, L135 (1993).
[16] C. O. Reinhold, D. R. Schultz, and R. E. Olson, J. Phys. B **23**, L591 (1990).
[17] R. Shingal, Z. Chen, K. R. Karim, C. D. Lin, and C. P. Bhalla, J. Phys. B **23**, L637 (1990).
[18] J. E. Miraglia and J. Macek, Phys. Rev. A **43**, 5919 (1991).
[19] K. Taulbjerg, J. Phys. B **23**, L761 (1990).
[20] C. P. Bhalla and R. Shingal, J. Phys. B **24**, 3187 (1990).
[21] R. E. Olson, C. O. Reinhold and D. R. Schultz, J. Phys. B **23**, L455 (1990).
[22] D. R. Schultz and R. E. Olson, J. Phys. B **24**, 3409 (1991).
[23] C. W. Woods, R. L. Kauffman, K. A. Jamison, N. Stolterfoht, and P. Richard, Phys. Rev. A **13**, 1358 (1976).
[24] W. Mehlhorn, Z. Phys. **160**, 247 (1960).
[25] H. I. Hidmi, C. P. Bhalla, S. R. Grabbe, J. M. Sanders, P. Richard, and R. Shingal, Phys. Rev. A **47**, 2398 (1993).
[26] A. Itoh, T. Schneider, G. Schiwietz, Z. Roller, H. Platten, G. Nolte, D. Schneider, and N. Stolterfoht, J. Phys. B **16**, 3965 (1983); R. Mann, S. Hagmann, and L. Weitzel, Nucl. Instrum. Methods Phys. Res. B **34**, 403 (1988).
[27] F. Bordoni, Nucl. Instrum. Methods **97**, 405 (1971).
[28] C. P. Bhalla, in *Recombination of Atomic Ions*, Vol. 296 of *NATO Advanced Study Institute, Series B: Physics*, edited by W. G. Graham, W. Fritsch, Y. Hahn, and J. A. Tanis (Plenum, New York, 1992), p. 87.
[29] J. Macek, Nucl. Instrum. Methods Phys. Res. B **53**, 416 (1991).
[30] H. I. Hidmi, P. Richard, J. M. Sanders, H. Schöne, J. P. Giese, D. H. Lee, T. J. M. Zouros, and S. L. Varghese, Phys. Rev. A **48**, 4421 (1993).
[31] N. Stolterfoht, in *Topics in Modern Physics*, edited by I. A. Sellin (Springer-Verlag, Berlin, 1978), Chap. 5, p. 155; N. Stolterfoht, D. Schneider, D. Burch, H. Wieman, and J. S. Risley, Phys. Rev. A **49**, 5112 (1994).